JETIR.ORG ISSN: 2349-5162 | ESTD Year : 2014 | Monthly Issue
JOURNAL OF EMERGING TECHNOLOGIES AND INNOVATIVE RESEARCH (JETIR)
An International Scholarly Open Access, Peer-reviewed, Refereed Journal

The Effect of Jeffrey Fluid in Chemically Reacting Dissipative Flow Passing a Vertically Inclined Plate with a Porous Medium Filled in the Despite of Constant Heat Flux and Thermal Diffusion: A Finite Element Method

A. Krishna Rao
Lecturer in Department of Mathematics,
Government Degree College,
Chodavaram, Anakapalli District, India- 531036
Email: alaka999@gmail.com

Abstract
Using non-dimensional variables, the non-linear governing coupled partial differential equations are transformed into linear coupled partial differential equations. The dimensionless temperature, concentration, and velocity fields are solved using the finite element method. Also, plotted graphical illustrations to show the physical understanding of subject under the study of various flow parameters. The local skin friction, rate of mass and heat transfer coefficients are produced in non-dimensional form and analysed using tabular representations in the additional. Our findings are limited to the well-established solutions found in the body of current literature for viscous and incompressible fluids. Because of this, the finite difference technique outperforms the other analytical and numerical methods and is stable and convergent.

1. Introduction:

The study of non-Newtonian fluids has established great attention in modern technologies such as geothermal engineering, geophysical, astrophysical bio-fluid and petroleum industries. Several basic relations of non-Newtonian fluids have been considered in the literature due to its resourceful nature. Non-Newtonian fluids have gotten the thought of specialist due to their modern and designing applications, i.e. passing on of paper, plastics production, material industry, nourishment handling, wire and edge covering and development of organic liquids. Experimentally, it has been observed that blood can be treated as non-Newtonian fluid at low shear rates in small arteries. Many physiological systems are modelled for biological tissues as porous layers. There are several proposed non-Newtonian fluid models to describe the behaviour of these bio fluids. Among them Jeffrey fluid is the generalization of Newtonian fluid. In the existing literature, several scientists have studied Jeffrey fluid under different mechanical and thermal boundary conditions ([166]-[172]). Now, metallurgical 2procedures, such as drawing and retreating of copper wires which involve cooling strips of continuous filaments, the MHD effect is to improve the rate of cooling. Mansur and Ishak [173] studied the MHD boundary layer flow of a nano fluid numerically. Ahmed et al. [174] applied the linearization method to the study of radiation effects on MHD boundary layer convective heat transfer in a porous media with low pressure gradient. A number of researchers discussed the MHD effects on Jeffrey fluid. Hayat et al. [175] found the chain solutions of MHD Jeffrey fluid in a channel. Das et al. [176] discussed Jeffrey fluid with MHD and slip condition. Jena et al. [177] found heat generation effects on MHD Jeffery fluid through a porous medium. Imtiaz et al. [178] found the effects of heterogeneous and homogenous reactions on MHD Jeffrey fluid. Ahmad and Ishak [179] studied the effects of

viscous dissipation effects on a Jeffrey fluid with MHD. Different studies on MHD flow on physical situations were considered for an example in Refs. ([180] and [181]). Imran et al. [182] studied MHD fractional Jeffrey's fluid flow in the presence of thermo diffusion, thermal radiation effects with first order chemical reaction and uniform heat flux. Vajravelu et al. [183] presented the influence of free convection on the nonlinear peristaltic transport of Jeffrey fluid in a finite vertical porous stratum using the Brinkman model.

The study of Magnetohydrodynamic (MHD) convective flow of an electrically conducting fluid is of considerable interest in many metallurgical and metal-working processes due to its frequent occurrence in industrial technology and geothermal application, high-temperature plasmas applicable to nuclear fusion energy conversion, liquid metal fluids, and (MHD) power generation systems. Sahu and Rajput [184] studied the combined effects of thermal diffusion and chemical reaction on the steady free convection MHD flow through a porous medium bounded by an infinite vertical surface with constant heat flux using two-term perturbation method. Alam et al. [185] analyzed the similarity solutions for hydromagnetic free convective heat and mass transfer flow along a semi-infinite permeable inclined flat plate with heat generation and thermophoresis. Alam et al. [186] have presented a two-dimensional steady hydromagnetic mixed convection and mass transfer flow over a semi-infinite porous inclined plate in the presence of thermal radiation, variable suction and thermophoresis. Singh et al. [187] studied the effects of thermophoresis on hydromagnetic mixed convection and mass transfer flow past a vertical permeable plate with variable suction and thermal radiation. Rashad [188] analyzed the influence of radiation on MHD free convection from a vertical flat plate embedded in porous media with thermophoretic deposition of particles.

Seddeek [189] analyzed the effect of chemical reaction, variable viscosity, thermophoresis and heat generation/absorption on a boundary-layer hydromagnetic flow with heat and mass transfer over a heat surface. Mahanthesh et al. [190] reported the magnetohydrodynamic flow of nanofluid over a bidirectional non-linear stretching surface with prescribed surface heat flux. The three-dimensional mixed convective hydromagnetic boundary layer flow of Casson nanofluid studied by Rauf et al. [191]. Shehzad et al. [192] and Abbasi et al. [193] examined the Peristalsis in a curved channel with slip condition and copper-water nanofluid with temperature-dependent effective viscosity in the presence of a magnetic field. Bourich et al. [194] studied analytically and numerically the Soret effect on the onset of convection in a vertical porous layer subjected to uniform heat flux. The influence of Soret and Dufour effects on flow field in free convection boundary layer from a vertical surface embedded in a Darcian porous medium has been studied by Postelinicu [195]. Pal and Mondal [196] studied the MHD non-Darcy mixed convective diffusion of species over a stretching sheet embedded in a porous medium with non-uniform heat source/sink, variable viscosity and Soret effect. Thermophoresis particle deposition in a non-Darcy porous medium under the influence of Soret, Dufour effects studied by Partha [197]. Hayat et al. [198] examined the

Soret and Dufour effects in three-dimensional flow over an exponentially stretching surface with porous medium, chemical reaction and heat source/sink.

Motivated by the above said research work, in this paper, we investigated the combined effects of thermal diffusion and viscous dissipation on an unsteady magnetohydrodynamic free convection, heat and mass transfer, electrically conducting non-Newtonian Jeffrey fluid flow over on an vertically inclined surface taken in to the account with constant heat flux. This paper to extend the work of Sahu and Rajput [184] for non-Newtonian Jeffrey fluid and angle of inclination. The emerging set of governing non-linear partial differential are solved numerically using finite element method. The effects of different non-dimensional controlling parameters on velocity, temperature and concentration profiles, along with the skin-friction factor, Nusselt and Sherwood numbers, are discussed and presented through graphs and tables.

a ---- Momentum boundary layer thickness,

b ---- Thermal boundary layer thickness,

c ---- Solutal boundary layer thickness

2. Mathematical formulation:

The conduct of Jeffrey fluid stream of a gooey, incompressible, electrically directing fluid installed in a permeable medium possessing a semi-endless area of the space boundary by a vertically slanted endless surface with steady heath motion within the sight of a transversely forced magnetic field and heat dispersion (Soret) is studied. The organize framework and the physical model of the problem are appeared in Fig. 1. For this research work the following assumptions are made.

An organize system (x', y') is presented with hub along the length of the plate (vertical surface) in the upward vertical course and hub ordinary to the plate (vertical surface) towards the fluid region. The plate is exposed to a steady suction parallel to $y'-$ axis.

The wall is maintained at constant temperature (T'_w) and concentration (C'_w) higher than the ambient temperature (T'_∞) and concentration (C'_∞) respectively.

- A uniform magnetic field of greatness is connected ordinary to the plate. The transverse connected attractive field and attractive Reynold's number are thought to be little, with the goal that the initiated attractive field is unimportant.
- The fluid properties are thought to be consistent with the exception of the thickness in the body force term.
- An artificially responsive animal types is discharged from the vertical surface into a hydrodynamic stream field. It diffuses into the fluid, where it experiences a homogeneous compound response. The response is expected to happen completely in the stream.
- It is accepted that there is no connected voltage which infers the absence of an electric field.
- The fluid has consistent kinematic viscosity and steady heat conductivity, and the Business's estimation have been adopted for the flow.
- The Cauchy stress tensor, $\bar{S}$, of a Jeffrey's non-Newtonian fluid [199] takes the form as follows:

$$S = \frac{\mu}{1+\lambda}\left(\dot{\gamma} + \lambda_1 \ddot{\gamma}\right) \quad (1)$$

where μ is the dynamic viscosity, is the proportion of relaxation to retardation times, speck over an amount signifies the material time subordinate and γ is the shear rate. The Jeffrey's model gives a rich definition to recreating hindrance and unwinding impacts emerging in non-Newtonian polymer streams. The shear rate and angle of shear rate are additionally characterized as far as velocity vector, $\bar{V}$, as follows:

where $\dot{\gamma} = \nabla\bar{V} + \left(\nabla\bar{V}\right)^T$ (2)

and $\ddot{\gamma} = \frac{d}{dt}\left(\dot{\gamma}\right) + \left(\bar{V}.\nabla\right)\dot{\gamma}$ (3)

Under the assumptions made above, the governing partial differential equations for the fully developed magnetohydrodynamic free convective heat and mass transfer flow of a viscous, incompressible, electrically conducting, viscous dissipative and chemically reactive Jeffrey fluid are

Continuity Equation:

$$\frac{\partial v'}{\partial y'} = 0 \quad \textbf{(4)}$$

Momentum Equation:

$$v'\frac{\partial u'}{\partial y'} = \nu\left(\frac{1}{1+\lambda}\right)\frac{\partial^2 u'}{\partial y'^2} + g\beta(\cos\psi)(T'-T'_\infty) + g\beta^*(\cos\psi)(C'-C'_\infty) - \left(\frac{\sigma B_0^2}{\rho}\right)u' - \left(\frac{\nu}{K'}\right)u' \quad \textbf{(5)}$$

Energy Equation:

$$v'\frac{\partial T'}{\partial y'}=\left(\frac{\alpha}{\rho C_p}\right)\frac{\partial^2 T'}{\partial y'^2}+\frac{\nu}{C_p}\left(\frac{\partial u'}{\partial y'}\right)^2 \quad \textbf{(6)}$$

Species Diffusion Equation:

$$v'\frac{\partial C'}{\partial y'}=D\frac{\partial^2 C'}{\partial y'^2}+D_T\frac{\partial^2 T'}{\partial y'^2}-k_r'\left(C'-C_\infty'\right) \quad \textbf{(7)}$$

together with initial and boundary equations

$$\left.\begin{aligned} &u'=0,\quad \frac{\partial T'}{\partial y'}=-\frac{q}{\alpha},\quad C'=C_w' \quad \text{at} \quad y'=0\\ &u'\to 0,\quad T'\to T_\infty',\quad C'\to C_\infty' \quad \text{as} \quad y'\to\infty \end{aligned}\right\} \quad \textbf{(8)}$$

Eq. (5.4) gives $v'=$ **Constant (**$=-v_o$**, say)** **(9)**

where $v_o>0$ **and** v' **is the steady normal velocity of suction on the surface. Let us introduce the following dimensionless variables**

$$\left.\begin{aligned} &u=\frac{u'}{v_o},\ y=\frac{y'v_o}{\nu},\theta=\frac{\alpha v_0\left(T'-T_\infty'\right)}{q\nu},\phi=\frac{C'-C_\infty'}{C_w'-C_\infty'},M=\frac{\sigma B_0^2\nu}{\rho v_o^2},K=\frac{K'v_o^2}{\nu^2},\\ &Gr=\frac{\nu^2 g\beta q}{\alpha v_o^4},Gc=\frac{\nu g\beta^*(C_w'-C_\infty')}{v_o^3},\Pr=\frac{\nu\rho C_p}{\alpha},Ec=\frac{\alpha v_o^3}{qC_p\nu},Sc=\frac{\nu}{D},\\ &Sr=\frac{D_T q}{\alpha v_o(C_w'-C_\infty')},Kr=\frac{k_r'\nu}{v_o^2},\mathrm{Re}=\frac{v_o x'}{\nu} \end{aligned}\right\} \quad \textbf{(10)}$$

The above defined non-dimensionless variables in Eq. (10) into Eqs. (5) -(7), and we get

$$\left(\frac{1}{1+\lambda}\right)\frac{\partial^2 u}{\partial y^2}-\frac{\partial u}{\partial y}-\left(M+\frac{1}{K}\right)u+Gr(\cos\psi)\theta+Gc(\cos\psi)\phi=0 \quad \textbf{(11)}$$

$$\frac{1}{\Pr}\left(\frac{\partial^2\theta}{\partial y^2}\right)-\frac{\partial\theta}{\partial y}+Ec\left(\frac{\partial u}{\partial y}\right)^2=0 \quad \textbf{(12)}$$

$$\frac{1}{Sc}\left(\frac{\partial^2\phi}{\partial y^2}\right)-\frac{\partial\phi}{\partial y}+Sr\left(\frac{\partial^2\theta}{\partial y^2}\right)-Kr\phi=0 \quad \textbf{(13)}$$

with associated initial and boundary equations

$$\left.\begin{aligned} &u=0,\quad \frac{\partial\theta}{\partial y}=-1,\quad \phi=1 \text{ at } \quad y=0\\ &u\to 0,\ \theta\to 0,\ \phi\to 0 \text{ as } y\to\infty \end{aligned}\right\} \quad \textbf{(14)}$$

All the symbols are described in nomenclature. The mathematical declaration of the problem is currently finished and encapsulates the arrangement of Eqs. (11), (12) and (13) subject to boundary equations (14). For right down to earth constructing packages and the plan of substance designing frameworks, the neighbourhood pores and skin-rubbing, Nusselt wide variety (Rate of heat change coefficient) and Sherwood number (Rate of mass alternate coefficient) are imperative bodily parameters for this type of boundary layer flow. The Skin-friction on the plate, which in the non-dimensional form is given by

$$Cf=\left(\frac{1}{1+\lambda}\right)\frac{\tau_w'}{\rho v_o\nu}=\left(\frac{1}{1+\lambda}\right)\left(\frac{\partial u}{\partial y}\right)_{y=0} \quad \textbf{(15)}$$

The rate of heat transfer coefficient, which in the non-dimensional form in terms of the Nusselt number is given by

$$Nu = -x' \frac{\left(\frac{\partial T'}{\partial y'}\right)_{y'=0}}{T'_w - T'_\infty} \Rightarrow Nu\,\mathrm{Re}^{-1} = -\left(\frac{\partial \theta}{\partial y}\right)_{y=0} \quad \textbf{(16)}$$

The rate of mass transfer coefficient, which in the non-dimensional form in terms of the Sherwood number, is given by

$$Sh = -x' \frac{\left(\frac{\partial C'}{\partial y'}\right)_{y'=0}}{C'_w - C'_\infty} \Rightarrow Sh\,\mathrm{Re}^{-1} = -\left(\frac{\partial \phi}{\partial y}\right)_{y=0} \quad \textbf{(17)}$$

3. Method of Solution:

Finite Element Technique: The finite element method (Bathe [200] and Reddy [201]) has been employed to solve Eqs. (11) -(13) under boundary equations (14). Finite element method is broadly utilized for taking care of boundary value problems. The fundamental idea is that the entire space is partitioned into littler components of boundary measurements called ""“Finite Elements”.". From there on the area is considered as a collection of these components associated at an element number of joint called "Nodes". The idea of discretization is received here. Different highlights of the strategy incorporate looking for persistent polynomial, approximations of the arrangement over every component in term of nodal qualities, and gathering of component equations by forcing the between component progression of the arrangement and parity of the between component powers. It is the most adaptable numerical procedure in present day building investigation and has been utilized to think about various problem in heat exchange [202], fluid mechanics [203], chemical processing [204], rigid body dynamics [205] and many other fields. The method entails the following steps:

Step-1: Finite Element Discretization: The entire area is separated into a finite number of sub-spaces, which is known as the discretization of the space. Each sub-space is called a component. The accumulation of components is known as the finite-element mesh.

Step-2: Generation of the Element Equations:

- From the work, an ordinary component is disconnected and the variational detailing of the given problem over the commonplace element is developed.
- A surmised arrangement of the variational issue is expected and the component equations are made by substituting this arrangement in the above system.
- The element matrix, which is called stiffness matrix, is developed by utilizing the component addition capacities.

Step-3: Assembly of the Element Equations: The algebraic equations so received are assembled with the aid of forcing the bury element congruity equations. This yields a significant quantity of arithmetical equations called the global boundary element exhibit, which administers the whole area.

Step-4: Imposition of the Boundary Equations: On the assembled equations, the Dirichlet's and Neumann boundary equations (14) are imposed.

Step-5: Solution of Assembled Equations: The assembled equations so obtained can be solved by any of the numerical technique viz. Gauss elimination method, LU Decomposition method, etc.

3.1.: Variational formulation: The variational formulation associated with Eqs. (11) -(13) over a typical two-nodded linear element $(y_e,\ y_{e+1})$ is given by

$$\int_{y_e}^{y_{e+1}} w_1 \left[\left(\frac{1}{1+\lambda}\right)\frac{\partial^2 u}{\partial y^2} - \left(\frac{\partial u}{\partial y}\right) - Nu + Gr\,\theta(\cos\psi) + Gc\,\phi(\cos\psi) \right] dy = 0 \quad (18)$$

$$\int_{y_e}^{y_{e+1}} w_2\left[\frac{\partial^2\theta}{\partial y^2}-(\mathrm{Pr})\left(\frac{\partial\theta}{\partial y}\right)+(Ec)(\mathrm{Pr})\left(\frac{\partial u}{\partial y}\right)^2\right]dy=0 \tag{19}$$

$$\int_{y_e}^{y_{e+1}} w_3\left[\frac{\partial^2\phi}{\partial y^2}-(Sc)\left(\frac{\partial\phi}{\partial y}\right)-(Kr)(Sc)\phi+(Sc)(Sr)\left(\frac{\partial^2\theta}{\partial y^2}\right)\right]dy=0 \tag{20}$$

Where $N=M+\frac{1}{K}$ and w_1, w_2, w_3 are arbitrary test functions and may be viewed as the variation in u, θ and ϕ respectively. After reducing the order of integration and non-linearity, we arrive at the following system of equations

$$\int_{y_e}^{y_{e+1}}\left[\left(\frac{1}{1+\lambda}\right)\left(\frac{\partial w_1}{\partial y}\right)\left(\frac{\partial u}{\partial y}\right)+(w_1)\left(\frac{\partial u}{\partial y}\right)+N(w_1)u-(Gr)(w_1)(\cos\psi)\theta-(Gc)(w_1)(\cos\psi)\phi\right]dy$$
$$-\left[(w_1)\left(\frac{1}{1+\lambda}\right)\left(\frac{\partial u}{\partial y}\right)\right]_{y_e}^{y_{e+1}}=0 \tag{21}$$

$$\int_{y_e}^{y_{e+1}}\left[(\mathrm{Pr})(w_2)\left(\frac{\partial\theta}{\partial y}\right)+\left(\frac{\partial w_2}{\partial y}\right)\left(\frac{\partial\theta}{\partial y}\right)-(Ec)(\mathrm{Pr})(w_2)\left(\frac{\partial\bar{u}}{\partial y}\right)\left(\frac{\partial u}{\partial y}\right)\right]dy-\left[(w_2)\left(\frac{\partial\theta}{\partial y}\right)\right]_{y_e}^{y_{e+1}}=0 \tag{22}$$

$$\int_{y_e}^{y_{e+1}}\left[(Sc)(w_3)\left(\frac{\partial\phi}{\partial y}\right)+\left(\frac{\partial w_3}{\partial y}\right)\left(\frac{\partial\phi}{\partial y}\right)+(Kr)(Sc)(w_3)\phi-(Sc)(Sr)(w_3)\left(\frac{\partial w_3}{\partial y}\right)\left(\frac{\partial\theta}{\partial y}\right)\right]dy$$
$$-\left[(w_3)\left(\frac{\partial\phi}{\partial y}\right)+(Sr)(Sc)(w_3)\left(\frac{\partial\phi}{\partial y}\right)\right]_{y_e}^{y_{e+1}}=0 \tag{23}$$

3.2. Finite Element formulation: The finite element model may be obtained from Eqs. (21) -(23) by substituting finite element approximations of the form:

$$u=\sum_{j=1}^{2}u_j^e\psi_j^e,\ \theta=\sum_{j=1}^{2}\theta_j^e\psi_j^e,\ \phi=\sum_{j=1}^{2}\phi_j^e\psi_j^e \tag{24}$$

With $w_1=w_2=w_3=\psi_j^e\ (j=1,2)$, where u_j^e, θ_j^e and ϕ_j^e are the velocity, temperature and concentration respectively at the jth node of typical eth element $(y_e,\ y_{e+1})$ and ψ_i^e are the shape functions for this element $(y_e,\ y_{e+1})$ and are taken as:

$$\psi_1^e=\frac{y_{e+1}-y}{y_{e+1}-y_e}\quad\text{and}\quad\psi_2^e=\frac{y-y_e}{y_{e+1}-y_e},\ y_e\le y\le y_{e+1} \tag{25}$$

The finite element model of the equations for eth element thus formed is given by

$$\begin{bmatrix}[K^{11}] & [K^{12}] & [K^{13}]\\ [K^{21}] & [K^{22}] & [K^{23}]\\ [K^{31}] & [K^{32}] & [K^{33}]\end{bmatrix}\begin{bmatrix}\{u^e\}\\ \{\theta^e\}\\ \{\phi^e\}\end{bmatrix}+\begin{bmatrix}[M^{11}] & [M^{12}] & [M^{13}]\\ [M^{21}] & [M^{22}] & [M^{23}]\\ [M^{31}] & [M^{32}] & [M^{33}]\end{bmatrix}\begin{bmatrix}\{u'^e\}\\ \{\theta'^e\}\\ \{\phi'^e\}\end{bmatrix}=\begin{bmatrix}\{b^{1e}\}\\ \{b^{2e}\}\\ \{b^{3e}\}\end{bmatrix} \tag{26}$$

Where $\{[K^{mn}],[M^{mn}]\}$ and $\{\{u^e\},\{\theta^e\},\{\phi^e\},\{u'^e\},\{\theta'^e\},\{\phi'^e\}\ and\ \{b^{me}\}\}(m,n=1,2,3)$ are the set of matrices of order 2×2 and 2×1 respectively. These matrices are defined as

$$K_{ij}^{11}=\left(\frac{1}{1+\lambda}\right)\int_{y_e}^{y_{e+1}}\left[\left(\frac{\partial\psi_i^e}{\partial y}\right)\left(\frac{\partial\psi_j^e}{\partial y}\right)\right]dy,$$

$$K_{ij}^{12} = N\int_{y_e}^{y_{e+1}}\left[\left(\psi_i^e\right)\left(\psi_j^e\right)\right]dy,\quad M_{ij}^{12} = M_{ij}^{13} = 0,\quad K_{ij}^{13} = -\left[Gr + Gc\right](\cos\psi)\int_{y_e}^{y_{e+1}}\left(\psi_i^e\right)\left(\psi_j^e\right)dy\quad M_{ij}^{11} = \int_{y_e}^{y_{e+1}}\left(\psi_i^e\right)\left(\psi_j^e\right)dy,\quad K_{ij}^{21} = 0,$$

$$K_{ij}^{22} = \int_{y_e}^{y_{e+1}}\left[\left(\frac{\partial\psi_i^e}{\partial y}\right)\left(\frac{\partial\psi_j^e}{\partial y}\right)\right]dy,\ M_{ij}^{33} = \int_{y_e}^{y_{e+1}}\left(\psi_i^e\right)\left(\psi_j^e\right)dy,$$

$$K_{ij}^{23} = -(Ec)(\Pr)\int_{y_e}^{y_{e+1}}\left(\frac{\partial\overline{\psi}_j^e}{\partial y}\right)\left(\frac{\partial\psi_j^e}{\partial y}\right)\left(\psi_i^e\right)dy,\quad M_{ij}^{21} = M_{ij}^{23} = 0,\quad M_{ij}^{22} = \int_{y_e}^{y_{e+1}}\left(\psi_i^e\right)\left(\psi_j^e\right)dy,\quad M_{ij}^{31} = M_{ij}^{32} = 0,\ K_{ij}^{31} = 0,$$

$$K_{ij}^{32} = -(Sr)(Sc)\int_{y_e}^{y_{e+1}}\left(\frac{\partial\psi_i^e}{\partial y}\right)\left(\frac{\partial\psi_j^e}{\partial y}\right)dy + (Kr)(Sc)\int_{y_e}^{y_{e+1}}\left(\psi_i^e\right)\left(\psi_j^e\right)dy,\ K_{ij}^{33} = \int_{y_e}^{y_{e+1}}\left[\left(\frac{\partial\psi_i^e}{\partial y}\right)\left(\frac{\partial\psi_j^e}{\partial y}\right)\right]dy,$$

$$b_i^{1e} = \left[\left(\psi_i^e\right)\left(\frac{1}{1+\lambda}\right)\left(\frac{\partial u}{\partial y}\right)\right]_{y_e}^{y_{e+1}},\ b_i^{2e} = \left[\left(\psi_i^e\right)\left(\frac{\partial\theta}{\partial y}\right)\right]_{y_e}^{y_{e+1}},$$

$$b_i^{3e} = \left[\left(\psi_i^e\right)\left(\frac{\partial\phi}{\partial y}\right) + (Sr)(Sc)\left(\psi_i^e\right)\left(\frac{\partial\theta}{\partial y}\right)\right]_{y_e}^{y_{e+1}}$$

The whole domain is subdivided into two noded components. More or less, the finite element equation is composed for all components and afterward on get together of all the element equations we get a system of request 328×328. Subsequent to applying the given limit equations an arrangement of 320 equations stays for numerical arrangement, a procedure which is effectively released using the Gauss-Seidel strategy keeping up an exactness of 0.0005.A intermingling measure dependent on the relative distinction between the present and past cycles is utilized. At the point when these distinctions fulfil the ideal precision, the arrangement is expected to have been combined and iterative procedure is ended. The Gaussian quadrature is executed for unravelling the reconciliations. The code of the calculation has been executed in C-Program running on a PC. Superb assembly was accomplished for every one of the results.

4. Program Code Validation:

In order to check on the correctness of the numerical procedure utilized for the arrangement of the problem considered in the present study, it was verified by performing reproduction for numerical answers for the consolidated impacts of heat dissemination and substance response on the relentless free convection MHD course through a permeable medium boundary by a boundless vertical surface with steady heatth motion which are accounted for by Sahu and Rajput [184]. Tables 1, 2 and 3 demonstrate the determined qualities for Skin-contact, Rate of heatth and mass exchange coefficients for the present arrangement when $\alpha = 0$, $\lambda \to \infty$ and the outcomes are distributed by Sahu and Rajput [184]. Tables 1, 2 and 3 demonstrate an extremely decent simultaneousness between the results and this loans believability to the present numerical code.

Table-1. Comparison of present numerical results with analytical results of Sahu and Rajput [184] for different values of *Gr*, *Gc* and *K*.

Gr	Present Numerical Results Cf	Analytical Results of Sahu and Rajput [184] τ
5.0	5.498852162	5.474180
10.0	9.548851248	9.558880
15.0	14.422581015	14.439100
Gc	Present Numerical Results Cf	Analytical Results of Sahu and Rajput [184] τ
5.0	5.498852162	5.474180
10.0	7.419985645	7.424620

15.0	9.435518267	9.449300
K	Present Numerical Results Cf	Analytical Results of Sahu and Rajput [184] τ
0.1	3.01399457	3.014740
0.4	4.60888532	4.615880
0.7	5.16998543	5.176170

Table-2. Comparison of present numerical results with analytical results of Sahu and Rajput [184] for different values of *Ec*, Pr and *M*.

Ec	Present Numerical Results Cf	Analytical Results of Sahu and Rajput [184] τ
-0.01	5.199978524	5.209880
0.01	5.498852162	5.474180
0.05	6.000159885	6.002780
Pr	Present Numerical Results Cf	Analytical Results of Sahu and Rajput [184] τ
0.71	5.498852162	5.474180
3.00	2.079995463	2.086700
7.00	1.584472015	1.599660
M	Present Numerical Results Cf	Analytical Results of Sahu and Rajput [184] τ
1.0	6.478885012	6.468820
2.0	5.498852162	5.474180
3.0	4.218841001	4.222860

Table-5.3. Comparison of present numerical results with analytical results of Sahu and Rajput [184] for different values of *Sr*, *Sc* and *Kr*.

Sr	Present Numerical Results Cf Sh		Analytical Results of Sahu and Rajput [184] τ Sh'	
0.0	4.819922145	2.733548952	4.821830	2.742820
0.5	5.139940015	2.248850122	5.146530	2.259890
1.0	5.498852162	1.774112045	5.474180	1.780800
Sc	Present Numerical Results Cf Sh		Analytical Results of Sahu and Rajput [184] τ Sh'	
0.22	6.518840152	0.449662015	6.525790	0.457140
0.66	6.018522145	0.833562127	6.025210	0.844031

0.78	5.936650012	0.928411523	5.942040	0.936298
Kr	Present Numerical Results *Cf* *Sh*		Analytical Results of Sahu and Rajput [184] τ *Sh*′	
-0.02	6.715532015	0.074152218	6.727250	0.082293
0.05	6.618446012	0.178852115	6.624760	0.184482
1.00	5.498852162	1.774112045	5.474180	1.780800

Cf and *Sh* - Present Numerical results & $\tau$and Sh^* --Analytical results of Sahu and Rajput [184].

5. Results and Discussions:

In the previous sections, the coupled partial differential equations (11), (12) and (13) had been settled numerically utilising finite element method issue to the boundary equations given through (14). Graphical portrayals of the numerical consequences are represented in Figs. 2 to 18 to demonstrate the impacts of various numbers at the restriction layer circulate. In this examine, studies the effect of the influences of material parameters independently in order to unmistakably watch their separate effects for the rate, temperature and recognition profiles of the flow. Additionally, the numerical after effects of pores and skin-erosion coefficients, charge of health and mass pass coefficients as some distance as Nusselt quantity and Sherwood variety for my part had been visible thru graphically. Throughout numerical computations of the critical pace, secondary speed, temperature and fixation, the estimations of the Prandtl range had been picked for mercury (*Pr* = 0.025), air at 25 degrees centigrade and one atmospheric strain (*Pr* = 0.71), water (*Pr* = 7.00) and water at four degrees centigrade (*Pr* = 11.62). To pay attention consideration on numerical values of the effects received within the take a look at the estimations of Sc have been picked for the gases speak me to diffusing concoction sorts of maximum basic enthusiasm for air to be particular hydrogen (*Sc* = 0.22), helium (*Sc* = 0.30), water vapor (*Sc* = 0.60) and smelling salts (*Sc* = 0.78). To find out association of this issue, an infinite vertical plate was installed a boundary length inside the movement. Subsequently, the whole problem in a boundary limit was comprehended. Be that as it may, in the charts, a range savvy step removes Δy of 0.001 is utilized with. The speed, temperature, and focus will in general zero as y keep an eye on 6. This is valid for any estimation of y. Along these lines Thus, finite length was considered in this study.

Fig.2 exhibits the impact of Grashof number for heat exchange on the speed profiles by keeping different parameters are fixed. The Grashof number for health exchange implies the overall impact of the heat lightness power to the thick hydrodynamic power in the limit layer. Obviously, it is seen that there's an ascent in the speed because of the development of heat lightness constrain. Likewise, as Gr builds, the top estimations of the rate increments fast close to the permeable plate and later on rots without difficulty to the unfastened stream pace. The effect of Grashof range for mass pass is printed in Fig.3. The Grashof range for mass trade characterizes the share of the species lightness power to the thick hydrodynamic electricity. Not surprisingly, the fluid velocity increments and the pinnacle esteem is progressively unmistakable because of increment in the species lightness compel. The velocity move achieves a selected finest incentive within the location of the plate and after that diminishes as it should be to approach the loose move value. It is noticed that the velocity increases with increasing estimations of the Grashof number for mass alternate. The effect of the Magnetic discipline parameter is regarded in Fig. 4. It is visible that the velocity of the fluid declines with the expansion of the appealing discipline wide variety traits. The discount inside the speed as the Magnetic field parameter increments is seeing that the nearness of an attractive subject in an electrically main fluid presents a strength called the Lorentz force, which acts towards the move if the appealing subject is connected the typical way, as within the gift investigation. This resistive strength backs off the fluid velocity component as appeared in Fig. 4. The effect of Permeability parameter is exhibited within the Fig. 5. From this discern we see that, the velocity is increments with increasing estimations of K. Physically, these final results can be achieved when the openings of the permeable medium are probably unnoticed.

From Fig. 6, It is observed that the momentum boundary layer thickness will increase for the fluids with *Pr* < 1 and decreases for *Pr* > 1. The Prandtl number truely depicts the relationship between pressure diffusivity and heat diffusivity and henceforth controls the overall thickness of the energy and heat restrict layers. At the point whilst *Pr* is little, that is, *Pr* = 0.025, it is visible that the heatth diffuses without delay contrasted with the

velocity. This implies that for fluid metals the thickness of the thermal boundary layer is a lot extra than the velocity limit layer. Fig. 7 portrays the effect of Prandtl quantity at the temperature discipline. It is seen that a selection inside the Prandtl quantity activates decline within the temperature field. Likewise, temperature area falls all of the greater quick for water in contrast with air and the temperature bend is definitely directly for mercury, that's an increasing number of reasonable closer to change in temperature. From this notion it's mile's purpose that mercury is first-class to hold up temperature contrasts and can be applied proficiently within the research center. Air can supplant mercury, the adequacy of retaining up temperature adjustments are extensively less than mercury. Notwithstanding, air can be reasonably-priced substitute for commercial reason. This is in view that, both increment of kinematic viscosity or lessening of thermal conductivity prompts increment in the estimation of Prandtl variety. Consequently, temperature diminishes with increasing of Prandtl quantity. The effect of Schmidt quantity on velocity profiles has been illustrated in Fig. 8. It is seen that, whilst all other taking element parameters are held constant and Sc is accelerated it's far visible that the rate diminishes in most cases. Further, it is visible that as we flow some distance from the plate, the fluid pace goes down. Fig. 9 presentations fixation profiles ϕ versus y for distinct gases like hydrogen (*Sc* = 0.22), helium (*Sc* = 0.30), water vapor (*Sc* = 0.60) and alkali (*Sc* =0.78). It is accounted for that the effect of expanding estimations of Schmidt number is to decrease the attention profiles. This is predictable with the way that the expansion of Sc implies a lessening of atomic diffusivity D that effects in decline of fixation limit layer. Consequently, the convergence of species is higher for littler estimation of Sc and decrease for bigger estimation of Sc. Moreover, it's miles visible that close to the boundary the thickness of recognition restricts layer increments altogether with increasing recurrence however inverse sample is referred to a way from the plate. The effect of the gooey dispersal parameter i.e., the Eckert range on the speed and temperature are seemed in Figs. 10 and 11 separately. The Eckert quantity communicates the relationship between the kinetic energy in the go with the flow and the enthalpy. It embodies the conversion of kinetic power by way of work completed against the viscous fluid stresses. More noteworthy thick dissipative heatth reasons an ascent in the temperature just as the speed. This conduct is obvious from Figs. 10 and 11. Figs. 12 and 13 painting the rate and fixation profiles for numerous estimations of the Soret number. The Soret wide variety characterizes the effect of the temperature angles inciting massive mass dissemination impacts. It is seen that a diffusion inside the Soret range consequences in an increment in the speed and attention inside the restriction layer. Fig. 14 represents the conduct of speed profiles for various estimations of substance response parameter. It is relevant to specify that Kr > 0 relates to a ruinous compound response. It very well may be seen from the profiles that the speed decreases in the declining compound response in the limit layer. This is because of the way that the expansion in the rate of synthetic response rate prompts decrease of a force in a limit layer in declining concoction response. It very well may be seen from the profiles that the cross-stream speed lessens in the declining compound response.

Fig. 15 demonstrates a dangerous sort compound response in light of the fact that the fixation diminishes for expanding concoction response parameter which shows that the diffusion rates can be massively changed by chemical reaction. This is due to the fact that an expansion in the compound response causes the focus at the boundary layer to wind up slenderer which diminishes the grouping of the diffusing species. This abatement in the grouping of the diffusing species reduces the mass dispersion. The impact of point of tendency of the surface on the speed field has been outlined in Fig. 16. It is seen that as the point of tendency of the surface builds the speed field diminishes. The speed profile in the Fig. 17 decreases that rate of movement is altogether diminished with expanding of Jeffrey fluid parameter. Additionally, it is seen from this Fig. 17, the limit layer force thickness diminishes as increment of Jeffrey fluid parameter.

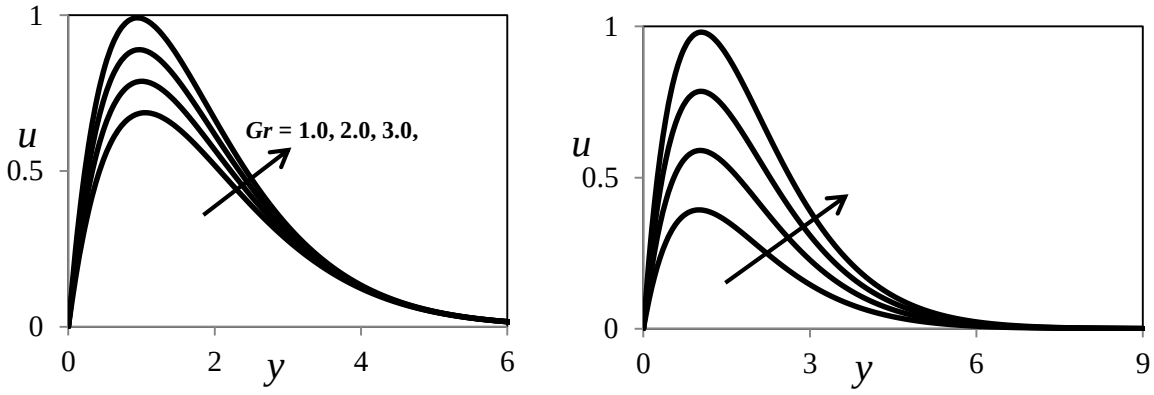

Fig. 2. Influence of *Gr* on Velocity Profiles

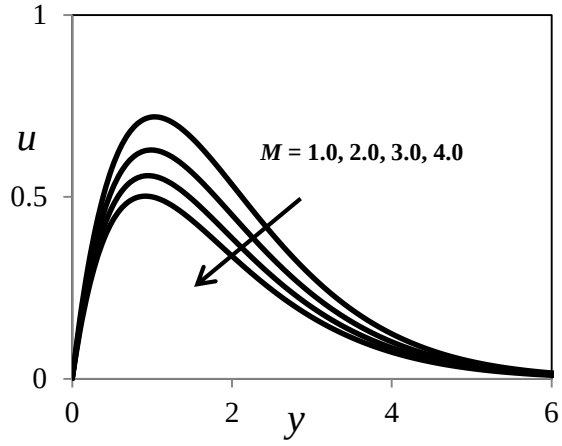

Fig. 3. Influence of *Gc* on Velocity Profiles

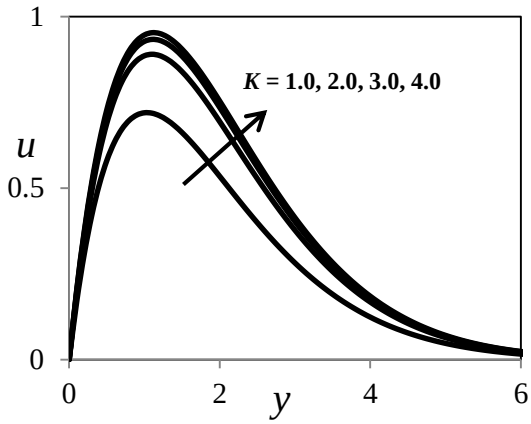

Fig. 4. Influence of *M* on Velocity Profiles

Fig. 5. Influence of *K* on Velocity Profiles

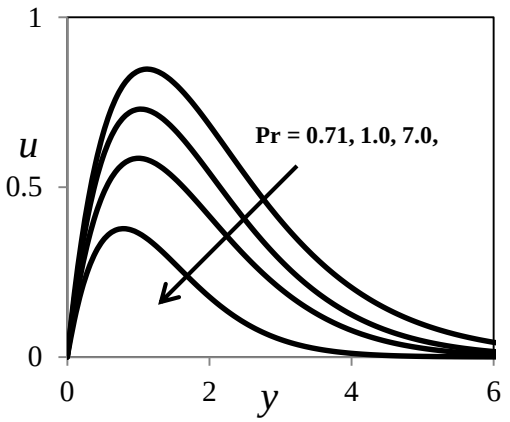

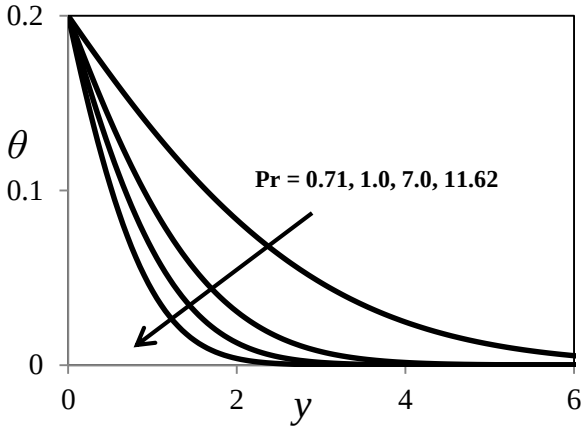

Fig. 6. Influence of *Pr* on Velocity Profiles

Fig. 7. Influence of *Pr* on Temperature Profiles

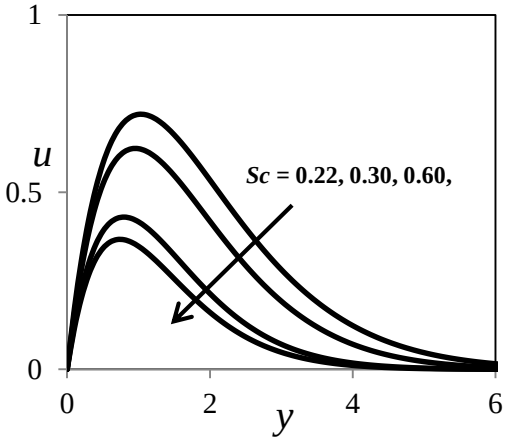

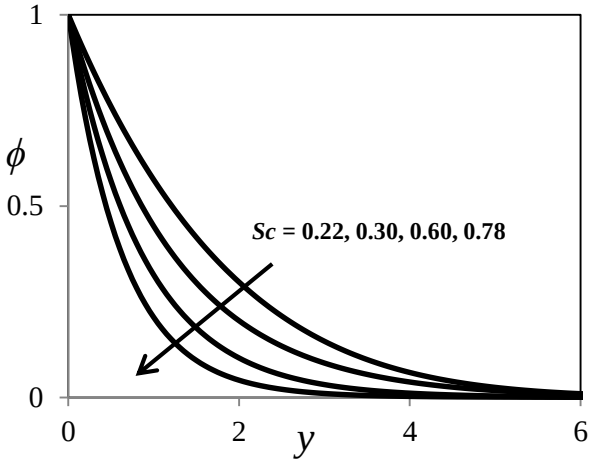

Fig. 8. Influence of *Sc* on Velocity Profiles

Fig. 9. Influence of *Sc* on Concentration Profiles

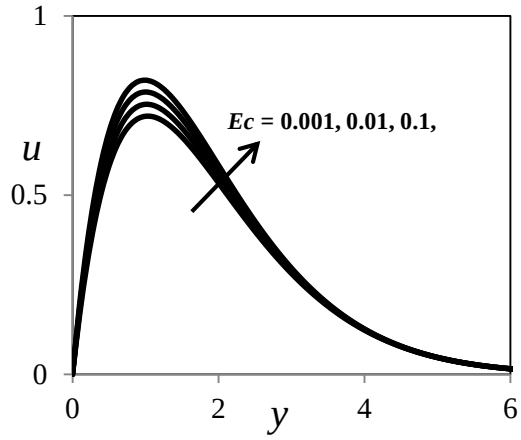

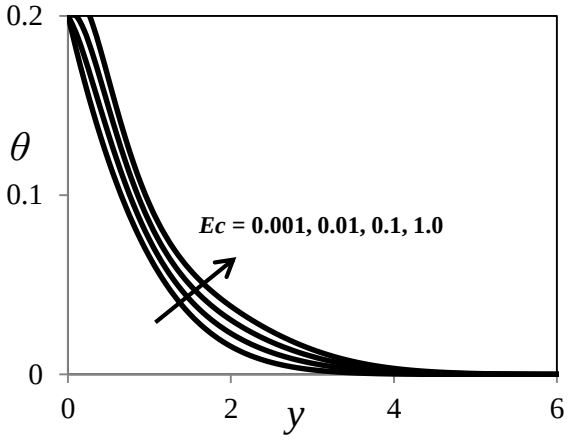

Fig.10. Influence of *Ec* on Velocity Profiles **Fig.11. Influence of *Ec* on Temperature Profiles**

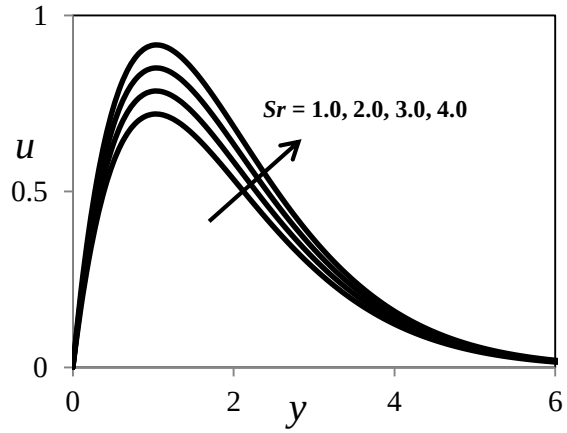

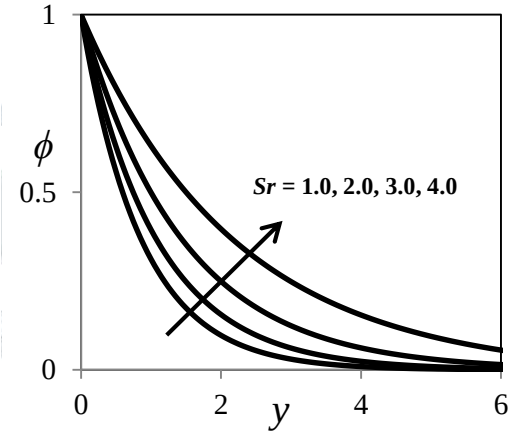

Fig.12. Influence of *Sr* on Velocity Profiles **Fig.13. Influence of *Sr* on Concentration Profiles**

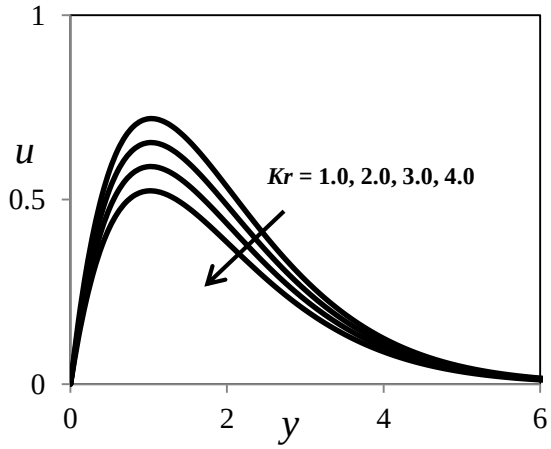

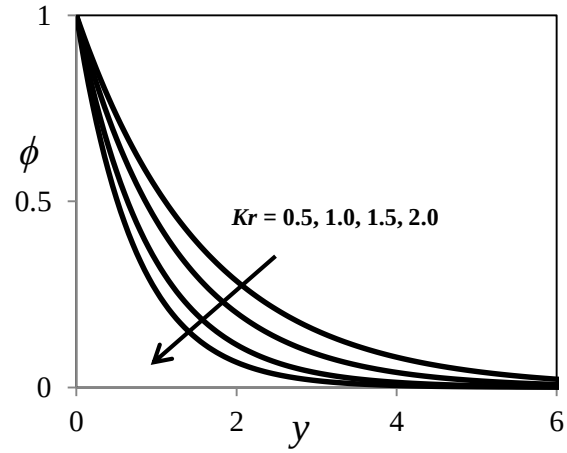

Fig.14. Influence of *Kr* on Velocity Profiles **Fig.15. Influence of *Kr* on Concentration Profiles**

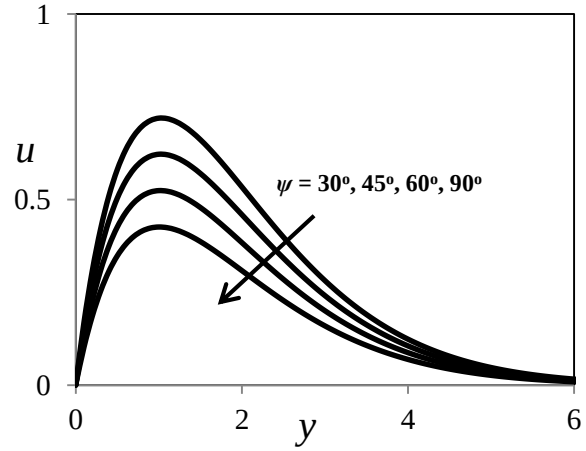

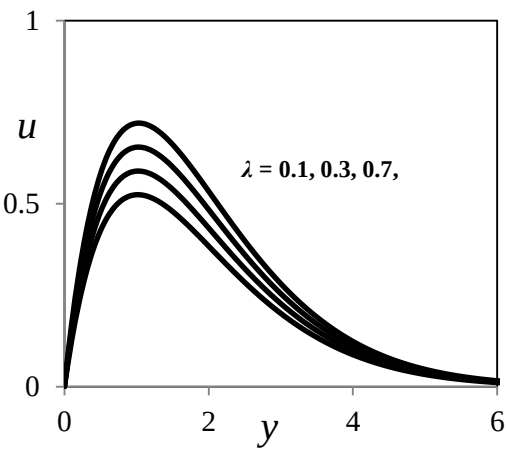

Fig. 16. Influence of ψ on Velocity Profiles **Fig. 17. Influence of λ on Velocity Profiles**

Table-4: Skin-friction values for different values of *Gr, Gc, M, K, Pr, Ec, Sc, Sr*, ψ, λ and *Kr*

Gr	*Gc*	*M*	*K*	Pr	*Sc*	*Sr*	*Ec*	ψ	λ	*Kr*	*Cf*
1.0	1.0	1.0	1.0	0.71	0.22	1.0	0.001	30^0	1.0	1.0	6.1244851254
2.0	1.0	1.0	1.0	0.71	0.22	1.0	0.001	30^0	1.0	1.0	6.3588102154
1.0	2.0	1.0	1.0	0.71	0.22	1.0	0.001	30^0	1.0	1.0	6.4012556921
1.0	1.0	2.0	1.0	0.71	0.22	1.0	0.001	30^0	1.0	1.0	5.9221542384
1.0	1.0	1.0	2.0	0.71	0.22	1.0	0.001	30^0	1.0	1.0	6.2511420075
1.0	1.0	1.0	1.0	7.00	0.22	1.0	0.001	30^0	1.0	1.0	5.9511200478
1.0	1.0	1.0	1.0	0.71	0.30	1.0	0.001	30^0	1.0	1.0	5.9633022147
1.0	1.0	1.0	1.0	0.71	0.22	2.0	0.001	30^0	1.0	1.0	6.2447811162
1.0	1.0	1.0	1.0	0.71	0.22	1.0	1.000	30^0	1.0	1.0	6.1544895001
1.0	1.0	1.0	1.0	0.71	0.22	1.0	0.001	45^0	1.0	1.0	6.0321812856
1.0	1.0	1.0	1.0	0.71	0.22	1.0	0.001	30^0	2.0	1.0	6.2114532689
1.0	1.0	1.0	1.0	0.71	0.22	1.0	0.001	30^0	1.0	2.0	6.0144785228

The impacts of different building administering parameters Grashof number for heat transfer, Grashof number for mass exchange, Magnetic field parameter, Permeability parameter, Prandtl number, Eckert number, Schmidt number, Soret number, Chemical reaction parameter, Angle of inclination parameter and Jeffrey fluid parameter on the skin-friction coefficient is appeared table 4. It is seen that as the Grashof number for heatth exchange, Grashof number for mass exchange, Permeability parameter, Soret number, Eckert number expands the skin-contact coefficient increments. It is discovered that as the Magnetic field parameter, Prandtl number, Schmidt number, Jeffrey fluid parameter, Chemical response parameter, Angle of tendency parameter expands the skin-friction coefficient decreases.

Table-5: Nusselt number and Sherwood number values for different values of *Pr, Sc, Ec, Kr* and *Sr*

Pr	*Ec*	*Nu*	*Sc*	*Sr*	*Kr*	*Sh*
0.710	**0.001**	**0.7441248662**	**0.22**	**1.00**	**1.00**	**0.6514885283**
7.000	**0.001**	**0.5844230154**	**0.30**	**1.00**	**1.00**	**0.4889521326**
11.62	**0.001**	**0.4145635821**	**0.22**	**2.00**	**1.00**	**0.8012445786**
0.710	**1.000**	**0.7885210145**	**0.22**	**1.00**	**2.00**	**0.5148820865**

In table 5, the effects of various engineering governing parameters Prandtl number, Schmidt number, Eckert number, Chemical reaction parameter and Soret number on the Nusselt and Sherwood number coefficients is studied. It is seen that as Eckert number increases the Nusselt number coefficient increments while it diminishes with expanding of Prandtl number. Additionally, it is discovered that as Soret number increases the Sherwood number coefficient increments while it decreases with increasing of Chemical reaction parameter and Schmidt number.